MODEL-BASED PARAMETER ESTIMATION IN ELECTROMAGNETICS: III--Applications to EM Integral Equations

E. K. Miller
3225 Calle Celestial, Santa Fe, NM 87501

0. ABSTRACT

Problem solving in electromagnetics, whether by analysis, measurement or computation, involves not only activities specific to these particular categories, but also some concepts that are common to all. Fields and sources are sampled as a function of time, frequency, space, angle, etc. and boundary conditions are satisfied through mathematical imposition or experimental conditions. The source samples, usually the unknowns in a problem, are found numerically or analytically by requiring them to satisfy both the appropriate form of Maxwell's Equations as relationships between them, together with the applicable boundary conditions. Alternatively, source samples may be measured under prescribed experimental conditions. These sampled relationships can be interpreted from the viewpoint of signal and information processing, and are mathematically similar to various kinds of filtering operations. It is this similarity that is discussed here in the context of model-based parameter estimation, where the dependence of electromagnetic fields and sources that produce them are both regarded as generalized signals.

MBPE substitutes the requirement of obtaining all samples of desired quantities (physical observables such as impedance, gain, RCS, etc. or numerical observables such as impedance-matrix coefficients, geometrical-diffraction coefficients, etc.) from first-principles models (FPMs) or from measured data (MD) by instead using a reduced-order, physically-based approximation, a fitting model (FM), to interpolate between, or extrapolate from, FPM or MD samples. When used for electromagnetic observables, MBPE can reduce the number of samples that are required to represent responses of interest, thus increasing the efficiency of obtaining them. When used in connection with the FPM itself, MBPE can decrease the computational cost of its implementation. Some specific possibilities for improving FPM efficiency are surveyed, specifically in terms of using FMs to simplify frequency and spatial variations associated with FPMs. Examples of MBPE applications are included here as well as speculative possibilities for their further development in improving FPM performance.

1.0 BACKGROUND AND MOTIVATION

The computational basis for solving most problems in physics and engineering, including computational electromagnetics (CEM) derives from first-principles mathematical descriptions, or first-principles models (FPMs), of the applicable physics. The computer models which derive from a FPM are developed using numerical analysis, a process that, as has been observed by Oppenheim and Schafer (1975), can be logically interpreted as generalized signal, or information, processing. Consider, for example, solving the LaPlace equation using finite differences, where $\nabla^2 V = 0 \approx (f_{i+1} + f_{i-1} - 2f_i)/h^2$ is equivalent to $f_i = (f_{i+1} + f_{i-1})/2$, showing that the potential at point i is the average of its neighboring values, with similar results obtained in two and three dimensions. Thus, the LaPlacian operator has the property of acting as a spatial, low-pass filter. More elaborate differential equations and numerical treatments produce different "computational molecules" or filters but ultimately lead to expressing a sample of an unknown from the applicable differential equation evaluated in terms of weighted sums of the unknowns in its neighborhood. In this sense, their computational molecules are equivalent to generalized spatial filters. Similar observations apply when solving integral equations numerically, but where the weighted sums that yield a sample of a specific unknown involve all other unknown samples.

Since numerical analysis does exhibit properties in common with signal processing, and also considering that one of the most productive uses of EM fields is the transmission of information, it seems reasonable to inquire about whether there may be possible benefits of examining CEM from a signal-, or information-processing, perspective. As discussed in part I of this article [Miller (1995)], referred to hereafter as RI, EM observables, however obtained, are well-approximated, or exactly described, by series of complex exponentials or complex poles. When the independent variables in the exponential and pole series are the time-frequency transform pair, their sums yield transient waveforms and frequency spectra, while other independent variables (see Table I of RI) are associated with different kinds of observables. For convenience,

the terms waveform domain (WD) and spectral domain (SD), respectively, will be used as generic descriptions whatever are the actual observables given by the exponential and pole series.

Continuing the theme begun in RI, we denote the exponential and pole series as "fitting models" (FMs) whose unknown coefficients are obtained numerically by their being "fitted" to samples of a FPM that they are intended to approximate and replace and which we denote as "generating models" (GMs). This procedure is known as model-based parameter estimation (MBPE). Although MBPE is discussed here specifically with respect to some representative EM applications and particular FMs, it should be appreciated that it is a very general procedure that is applicable to essentially any process, physical or otherwise, for which a reduced-order, parametric model can be deduced. Also, it must be noted that MBPE is not "curve fitting" in the sense that term is normally used, which also can involve finding the parameters of some function which is fit to the available data. The essential difference between MBPE and curve fitting is that the former uses a FM based on the problem physics, while the latter need not do so, which is why MBPE might be characterized as "smart" curve fitting. When curve fitting includes the goal of finding the correct FM for the process that generated the given data, this approach can also be described as "system identification." It's worth emphasizing that MBPE is not limited to physical processes but forms the basis for variously named analytical procedures {e.g., Kummer's method, Richardson extrapolation and Romberg quadrature [Ralston (1965)]} whose purpose is to speed the numerical convergence of mathematical representations involving integrals and infinite sums and wherein the integrand function or the sequence of partial sums can be regarded as a generalized "signal." In discussing a non-linear procedure he developed for a similar purpose, Shanks (1955) referred to such phenomena as "physical" and "mathematical" transients. In essence, any process that produces a sequence or set of samples is a candidate for MBPE.

In the first part of this article, RI [Miller (1995)], the mathematical background of MBPE is presented for WD and SD signals, showing that the associated FMs can be quantified using function sampling, derivative sampling, or a combination thereof. The second part, RII [Miller (1996)] demonstrates use of MBPE for developing approximate, reduced-order representations of a variety of EM observables in the WD and SD, an example of which is included in this special issue [de Beer and Baker (1995)]. In this article we discuss application of MBPE to improving the computational efficiency of a FPM.

2.0 MBPE APPLICATION TO A FREQUENCY-DOMAIN INTEGRAL-EQUATION, FIRST-PRINCIPLE MODEL

Almost all EM boundary-value problems involve finding the fields over some surface or throughout some volume due to sources distributed over that same surface or volume. When using an integral-equation formulation, these source-field relationships are given by a Green's function or some equivalent field propagator, whereas a differential-equation model employs the Maxwell curl equations as the propagator. The spatial behavior of the fields might be viewed for some purposes as a generalized signal, as can angle, time and frequency dependencies of such fields as well. Such a perspective can suggest alternate ways of representing the fields in signal-processing terms for numerical purposes to simplify whatever computations that must be done, a viewpoint that is explored here.

For moment-method models based on a frequency-domain integral equation (FDIE) (other FPMs can be analyzed in a similar context), the number of arithmetic operations or operation count (OC), required for solution at a single frequency f_i, OC_i, will depend on the number of unknowns, X_{si}, used in the model approximately as

$$OC_i \sim A_X X_{si}^2 + B_X X_{si}^3 \tag{1a}$$

or, in terms of frequency, f, as

$$OC_i \sim A_f f_i^4 + B_f f_i^6 \tag{1b}$$

for a three-dimensional object requiring two-dimensional sampling (i.e., sampling over its surface). When a solution is desired over some frequency interval, as is usually the case, then the total operation count, OC_T, can be estimated as

$$OC_T \sim \Sigma A_f f_i^4 + B_f f_i^6,\ i = 1, \ldots, F \tag{2}$$

where there are a total of F solution frequencies.

The "A" terms here account for filling the "system" matrix [known as the impedance or $\underline{\underline{Z}}$ matrix when an electric-field integral equation (EFIE) is used], and the "B" terms account for solving the system matrix in factored or inverted form as a "solution" matrix (known as the admittance or $\underline{\underline{Y}}$ matrix when using an EFIE). Use of iterative solution techniques changes the above B terms to $B'_X X_{si}^2$ and $B'_f f_i^4$ but where B_f' can be much larger than B_f. Various, so-called "fast"techniques are being developed with the goal of

reducing the highest-order terms in Eq. (1a) to of order $X_{si}\log(X_{si})$. Clearly, any means of reducing F would also be helpful in decreasing the total computational cost, a point that is considered in detail in Sections 4 and 5. First, let's consider how the impact on OC_i of the individual terms in Eq. (1) can be mitigated.

It can be observed that as the frequency increases from zero for a given problem, OC_i at first grows in proportion to FX_i^2 or Ff_i^4, but it eventually becomes proportional to FX_i^3 or Ff_i^6 when the higher-order term begins to dominate, assuming a constant spatial sampling density per λ^2. By reducing both the number of impedance matrices that need to be computed from the defining formulation when impedance-matrix computation dominates OC_i, and the number of admittance matrices that need to be solved from the impedance matrix when solution time dominates OC_i, it should be possible to significantly reduce the OC_T required to cover a specified bandwidth. This might be done by modeling the frequency behavior of the impedance matrix for smaller problems, and the frequency behavior of the admittance matrix for larger problems, in both cases with the goal of reducing the number of FPM evaluations needed, i.e. to reduce F in Eq. (2), and to thus minimize OC_T. It should be noted that the "crossover" point in X_{si} between fill-time and solution-time domination of OC_i, can vary from as few as 200 unknowns to as many as 10,000 unknowns. Thus, the $\underline{\underline{Z}}$ and $\underline{\underline{Y}}$ matrices, or their interaction coefficients, both become candidates for MBPE, albeit using different kinds of FMs as is considered below.

In addition to modeling the frequency behavior of $\underline{\underline{Z}}$ and $\underline{\underline{Y}}$, it is also worth considering whether the spatial behaviors of either of these matrices can be modeled. From a signal-processing perspective, the spatial variation of the field over an object due to a given localized source (e.g., a subdomain basis function) on that object might be regarded as a generalized signal. If this field "signal" can be predicted or estimated using a FM that is computationally simpler than using the defining equations normally employed for calculating the exact interaction coefficients, the magnitude of the A_f term in Eq. (2) could be commensurately reduced. Alternatively, if a first-principles evaluation of only a subset of the X_s^2 interaction coefficients needs to be done, say CX_s where $C << X_s$, and the rest can be estimated from the rigorously computed coefficients, then the effect would be to change the $A_xX_s^2$ term to of order CA_xX_s, if the cost of obtaining the estimated values is much less than that of the rigorously computed coefficients.

A specific example of reducing the A_f term in Eq. (2) is to compute none of the X_s^2 interaction coefficients in $\underline{\underline{Z}}$ from first principles, but instead to estimate them using some appropriate FM based on a small set of precomputed, first-principles field samples. This approach, summarized in Section 4 below, was used by Burke and Miller (1984) for reducing the cost of evaluating the Sommerfeld integrals that arises when modeling objects near an interface where the FMs are analytical approximations to these integrals. Their approach is an extension of earlier work described by Miller et al. (1977) where linear interpolation of sampled Sommerfeld integrals for the matrix coefficients was used as a curve-fitting procedure rather than MBPE. Other problems having special Green's functions are also candidates for this procedure, another example of which is provided by modeling sources between infinite parallel planes [Demarest et al. (1989)]. In these instances, the reduction in OC_i is reflected in a decrease in the A_f coefficient in Eq. (1).

Another way of reducing the effect of the A_f term is to exploit the fact that, as the source and observation points become more widely separated, the complexity of their interaction fields is reduced. This is easy to see by considering that the fields in the vicinity of a linear source distribution of a few wavelengths in extent are to be pointwise sampled along a line parallel to, and a distance ε away from, the source. In order to develop an accurate-enough representation, it would necessary to sample the field at some minimum density per wavelength. Now consider the situation as the sampling line is moved further and further away from the source. The field variation along that line will become less complex as the near-field components decrease with increasing distance and finally only the 1/r field remains. Furthermore, with increasing observation distance, the spatial variation of the field along a line of fixed length further decreases in complexity because the angle subtended by this line at the source monotonically decreases. In other words, at a great enough, finite distance away from the source, the field variation becomes a function of subtended angle rather than of linear distance over some fixed observation range.

Thus, the effective rank of the interaction between sources of given size decreases as their separation distance increases, reducing the complexity of that interaction, and, consequently, the amount of computation needed to determine it to some specified

accuracy. This idea is exploited in techniques such as the fast multipole method [Coifman, et al. (1993)], impedance-matrix localization [Canning (1990)], recursive models [Chew (1993)], etc., where rank reduction is explicitly employed, or where more distant interaction coefficients are approximated by simpler expressions [Vecchi et al. (1993)]. Such approaches effectively employ exact interaction coefficients when the source and observations points are close and controlled approximations as their separation distance increases. This results in an A_f coefficient that becomes smaller as source-observation distance increases, or a reduced matrix-fill time. In addition, because the interaction complexity decreases with increasing distance for fixed source and observations spans, the complexity, or effective number of interaction coefficients also decreases, reducing the OC_i of multiplying the impedance matrix by a source vector from of order $(X_i)^2$ to of order X_i. The OC_i associated with solving a matrix having X_i unknowns by iteration thus trends towards order X_i or $X_i \log X_i$ from being of order $(X_i)^2$.

Whether spatial variations in the solution or admittance matrix might be exploited in a similar fashion is not so clear. Certainly, a valid solution to the original problem must exhibit spatial dependencies consistent with the geometry and excitation involved and be consistent with Maxwell's equations. Graphical examination of the $\underline{\underline{Y}}$ matrix for simple objects like a straight wire[Miller et al. (1981) and below] reveals that it exhibits a standing-wave character, not a surprising result in that the currents on such structures are well-known to have such behavior. In other words, the "traveling-wave" nature of the Green's function in the formulation domain, reflected in terms like exp(ikR)/R, is converted to a standing-wave response in the solution domain, where amplitude maxima occur at resonances associated with the object poles. Thus, an appropriate FM for the admittance matrix should apparently be expected to be of wave-domain type as well. These kinds of ideas are now explored from the perspective of MBPE in the following section.

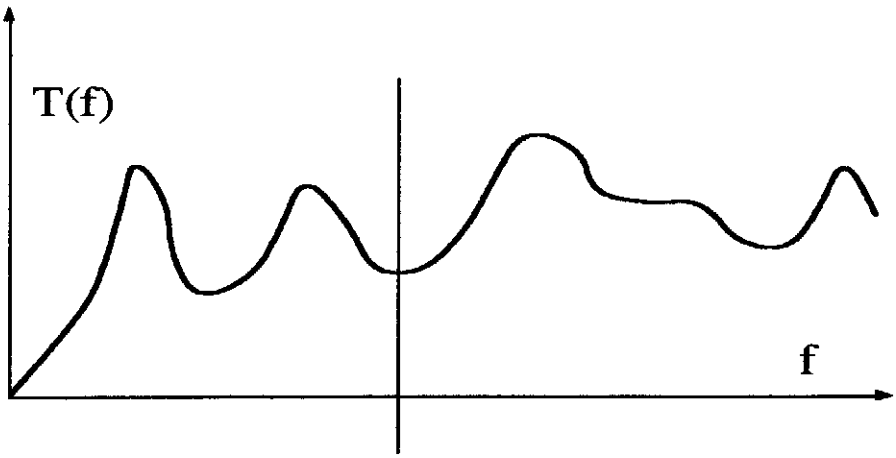

$A_{fill} f^4 > B_{solve} f^6$

Formulation-domain modeling:
reduce complexity of coefficient computation and minimize number of matrix-fill frequencies.

$A_{fill} f^4 < B_{solve} f^6$

Solution-domain modeling:
reduce cost of matrix solution and minimize number of matrix-solution frequencies.

Figure 1. Illustration showing where matrix-fill and matrix-solution operation counts dominate for a frequency-domain integral equation solved using L-U decomposition and assuming that a fixed sampling density per wavelength is used as frequency is increased. At lower frequencies a computational benefit can be realized by finding ways to compute interaction coefficients more efficiently or to reduce the number of rigorously computed $\underline{\underline{Z}}$ matrices. At higher frequencies, a computational benefit results from reducing the number of solutions, or $\underline{\underline{Y}}$ matrices.

3.0 THE TWO APPLICATION DOMAINS IN INTEGRAL-EQUATION MODELING

We have discussed MBPE in CEM from the perspective of whether the quantities of interest exhibit wavelike or polelike behavior, referring to their respective occurrences by the designations waveform domain and spectral domain, respectively, determined by the mathematical description that applies to a given quantity. There is another domain pair that is also useful for problem categorization, one describing the

domain wherein a boundary-value problem is defined, and the other describing the domain wherein a solution to that problem is presented. We refer to the former as the "formulation" domain, in which a formal mathematical statement originating from Maxwell's Equations is developed for a problem, and to the latter as the "solution" domain, in which that original formulation has been mathematically solved. In the formulation domain we begin with known exciting fields to which to-be-found induced sources are required by Maxwell's Equations to satisfy the appropriate boundary conditions. Finding these induced sources requires inverting the original source-field relationship. For all but the simplest problems the inversion requires numerical computation.

A potential approach to alleviating the computational requirements that arise in either the formulation domain or solution domain is to exploit the underlying physical and mathematical behavior of EM fields, as is embodied in first-principles analysis of wave-equation problems, through a simplifying, reduced-order, signal-processing formalism. Of course, knowledge of the problem physics is required to begin with as any solution process, analytical or numerical, can not be initiated without having the applicable physics captured in appropriate mathematical form, something that in terms of Maxwell's Equations might be characterized as a microscopic description. But the physical behavior of greater practical interest is usually macroscopic in nature, as it is not generally the fine details of the current distribution on an antenna or the near fields around a scatterer, but the antenna input impedance and gain, or scattering cross section, that are needed for system design. The macroscopic description is naturally a reduced-order one and provides the context for MBPE.

As previously observed, MBPE involves fitting physically motivated analytical approximations (the model) to accurately computed or measured EM observables from which unknown coefficients (the model parameters) are numerically obtained. These fitting models can then be used in subsequent applications to more efficiently characterize time, frequency, angle and space responses as well as to provide more insightful access to the underlying physics. In the solution domain, MBPE can be applied directly to the spatial and frequency dependencies of the computed observables themselves, such as currents and fields as discussed in RII, or instead to the solution matrix from which these quantities are obtained, as is discussed here.

Alternatively, we might also employ MBPE in the formulation domain, where it is the behavior of the first-principles analytical representation that is being approximated by reduced-order FMs. In that case, the frequency and space dependence to be represented would be that of the defining source-field relationships as contained in the system matrix. In contrast to working in the solution domain, where resonance effects dominate the EM behavior, growing phase change and geometric attenuation of the fields of increasingly distant sources dominate the behavior when working in the formulation domain. While the most appropriate FM will depend on the particular quantity being modeled, exponential- and pole-series models are widely applicable. For example, the frequency and spatial variations of a FDIE are suitable for exponential, or WD, FMs in the formulation domain, whereas in the solution domain pole-series FMs are suitable for frequency and angle variations and exponential-series FMs for their spatial variation. Formulation-domain approaches are described by Newman (1988) and Benthien and Schenck (1991), and solution-domain approaches are presented in Burke et al. (1988, 1989). Other kinds of FMs can be found useful, e.g. based on the geometrical theory of diffraction, for other analytical formulations and solutions. Some of these possibilities are discussed in the following sections. Each of these two FMs and problem domains are considered in the following.

4.0 FORMULATION-DOMAIN MODELING

4.1 Waveform-Based MBPE in the Formulation Domain

The question to be considered here is how waveform-based MBPE might be used for improving the numerical solution of a FDIE. First observe that the coefficients that appear in the impedance matrix for an FDIE model can be expressed in the generic form

$$Z_{m,n}(\omega) = \int_{\Delta_n} S_n(\omega) K_{R,m,n}(\omega) K_{\Delta,m,n}(\omega) d\Delta_n \tag{3}$$

where m and n denote the observation and source patches, respectively; S_n is the source on patch Δ_n; $K_{R,m,n}$ is the patch-to-patch (or P-P) part of the IE kernel; and $K_{\Delta,m,n}$ is the in-patch (or I-P) part of the kernel, where we have assumed a subdomain numerical model is being used. These terms refer, respectively, to that part of the kernel function whose frequency and spatial dependence is driven by an exponential phase change due to the P-P distance as contrasted with those variations due to variable positions within the source (and, possibly, observation) patches. Because increasing the P-P distance and increasing the frequency both increase the phase of $K_{R,m,n}$, changes in one or the other of these variables have similar effects on interaction phase, an effect that is exploited in using scale models in making

experimental measurements. Considering frequency variations specifically, except for the patches that are close to each other (with respect to the wavelength), the P-P term would normally represent a faster frequency variation while the I-P would always represent a slower frequency dependence because patches need to be small relative to a wavelength while the interpatch distance can be arbitrarily large. The $X_S x X_S$ set of interaction coefficients defined by Eq. (3) provides all the information needed to represent an object's EM characteristics, to the degree permitted by a numerical model based on it, but the source-field, integral-equation relationship represented by $\underline{\underline{Z}} \cdot \underline{I} = \underline{V}$ must be inverted to $\underline{I} = \underline{\underline{Y}} \cdot \underline{V}$ to obtain the desired solution.

The P-P, or fast, term always has the form, for IE-based models,

$$K_{R,m,n}(\omega) = e^{jkr_{m,n}}/r_{m,n} \tag{4}$$

where $r_{m,n}$, the separation between the origins of the source- and observation-patch local coordinates, is assumed to be a far-field distance and k is the wavenumber, a form that emphasizes the traveling-wave nature of the impedance-matrix coefficients. Integration over the source patch (and, possibly, the observation patch if using other than delta-function field sampling; though here we explicitly consider only source integration) involves changes in the fast term of order $\exp(jk\Delta r_{mn})$, where $k\Delta r_{mn} \ll 1$ is the distance variation caused by scanning over patch n. The interaction coefficient $Z_{m,n}$ can, thus, be rewritten as

$$Z_{m,n}(\omega) = e^{jkR_{m,n}} \int_{\Delta_n} S_n(\omega) K'_{\Delta,m,n}(\omega) d\Delta_n \tag{5}$$

with $R_{m,n} + \Delta r_{mn} = r_{m,n}$ and $K_{\Delta,m,n}$ a modified slow-variation kernel. This form of interaction coefficient suggests that we can estimate $Z_{m,n}(\omega_2)$ at a new frequency ω_2 from an accurately computed value at frequency ω_1 as

$$Z_{m,n}(\omega_2) \approx Z_{m,n}(\omega_1) e^{j(\omega_2-\omega_1)(R_{m,n}/c)} M_{m,n}(\omega_2-\omega_1) \tag{6}$$

where $M_{m,n}(\omega_2-\omega_1)$ is an interpolation model that accounts for the slowly varying part of the kernel function whose specific form would depend not only on object geometry but on whatever frequency dependence might have been incorporated into the basis and testing functions that are used. Exploiting a capability for modeling the spatial variation and its decreasing complexity with increasing distance is more involved, but is essentially embodied in "fast" methods which seek to reduce the OC of filling $\underline{\underline{Z}}$ and performing $\underline{\underline{Z}} \cdot \underline{I}$ multiplies from of order X_S^2 to of order $X_S \mathrm{Log}(X_S)$ [e.g., see Canning (1990), Chew (1993), Coifman et al. (1993)]. The specific problem of modeling the frequency variations in $\underline{\underline{Z}}$ is considered next.

4.1.1 Modeling Frequency Variations--Antenna Applications. The model $M_{m,n}$ might be represented in various ways including using low-order polynomials (the model) whose coefficients (the parameters) are computed from samples of $Z_{m,n}$ at selected frequencies [Newman (1988), Benthien and Schenck (1991)]. When sinusoidal bases functions specifically are used, it may also be advantageous to develop a recursive form for $M_{m,n}$. By accurately computing the impedance matrix at widely spaced frequencies and using estimated values at intervening frequencies, the goal is to obtain acceptably accurate results across a wide bandwidth without the cost of computing the impedance matrix at all sampling frequencies desired. As an example application, the analytical behavior of the impedance-matrix coefficients has been approximated for small variations in frequency about the computation point ω_1 by [Newman (1988)]

$$M_{m,n}(\omega - \omega_1)|_{imag} = A_i + B_i \ln(\omega - \omega_1) + C_i(\omega - \omega_1) \tag{7}$$

$$M_{m,n}(\omega - \omega_1)|_{real} = A_r + B_r(\omega - \omega_1) + C_r(\omega - \omega_1)^2 \tag{8}$$

A result obtained by Newman is presented in Fig. 2 where the input impedance of a center-fed dipole antenna is plotted as a function of frequency over its first two resonance frequencies. Two different curves are shown, one for a GM sample interval of 300 MHz and the other of 600 MHz.

Virga and Rahmat-Samii (1995) used $\underline{\underline{Z}}$-matrix frequency modeling for more complex communications antennas, one result for which is shown in Fig. 3. There the input impedance of a 4-turn helical antenna on an infinite ground plane is plotted versus frequency as obtained by direct evaluation and from two interpolation methods. The interpolated results are obtained using a simple quadratic FM and a second FM that incorporates the singularity of interaction coefficients for segments closer than one-half

wavelength and otherwise uses Eqs. (6) to (8). The authors report an approximately 30-to-1 computer savings results from modeling the $\underline{\underline{Z}}$ matrix as compared with direct evaluation at a total of 301 frequency samples.

4.1.2 Modeling Frequency Variations: Elastodynamic Scattering. Benthien and Schenck (1991) have used an approach similar to the above for modeling elastodynamic problems whose frequency responses, it should be noted, can be much more complex in structure than typical EM spectra. One interesting aspect of their work is that they are able to span a bandwidth that includes several resonances with only two FPM system-matrix computations at its endpoints while using MBPE for frequencies between them, in contrast to modeling the solution (admittance) matrix where the equivalent of two samples per resonance are required [RII]. The resonance structure is manifested only when the solution has been developed, or the source-field description has been inverted. This difference stems from the fact, so long as phase changes are handled accurately enough across a given frequency interval over which the phasor between the most widely spaced points on the object being modeled rotates through several (say n) times 2π, then n to 2n resonances can be predicted by using only 2 FPM samples. Examples of Benthien and Schenck's results are included in Figs. 4 and 5.

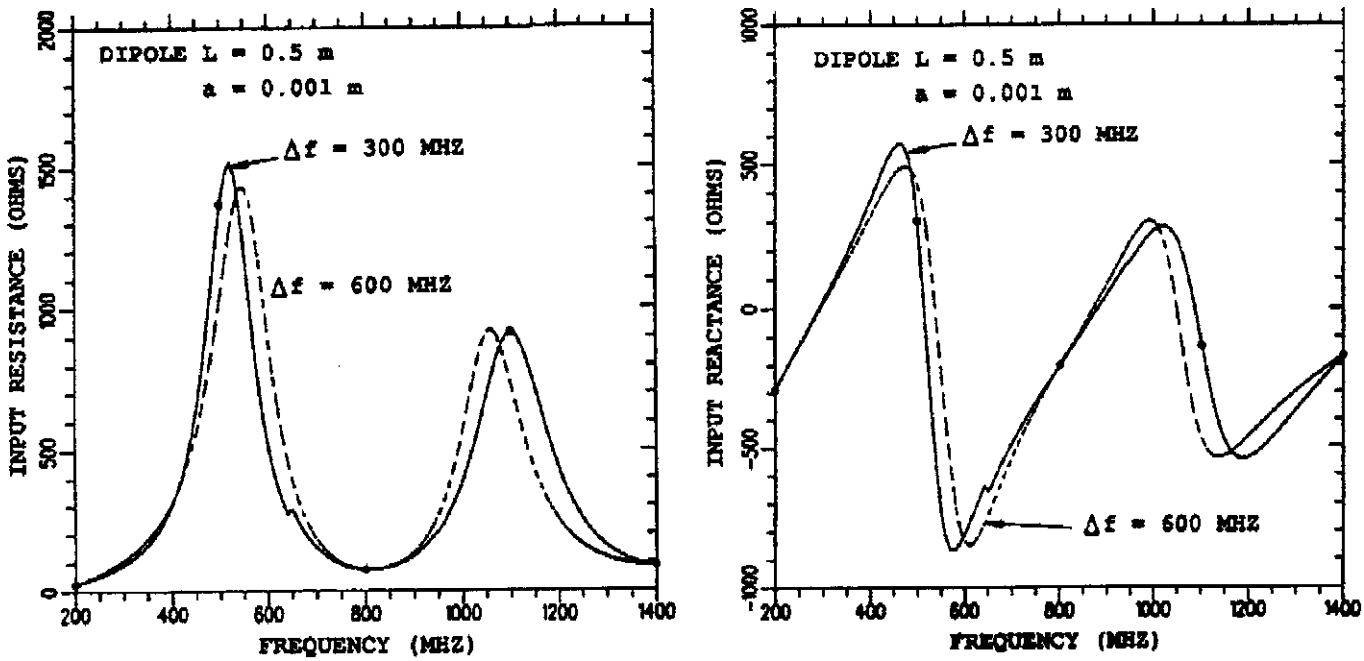

Figure 2. Results from using MBPE and two different FMs to represent the interaction coefficients of the $\underline{\underline{Z}}$ matrix of a center-fed, half-wave dipole antenna [Newman (1988)]. The FMs employ the approach of Eqs. (31) to (33) and are based on GM samples spaced 300 MHz apart (the solid line) and 600 MHz apart (the dashed line). The discontinuity in the impedance curves occurs at the point where a FM replaces a GM sample at one end of its span with a new one at the other as successive GM samples are employed.

4.1.3. Modeling Spatial Variations: The Sommerfeld Problem. A computationally demanding problem is that of determining the Sommerfeld fields that result from the interaction of elementary sources with a half space and which become part of the Green's function in an IE model for antennas near ground, microstrip structures, etc. One of the first approaches to this problem to incorporate numerically the rigor of the Sommerfeld integrals while avoiding their computational complexity used a two-dimensional mesh of pre-computed Sommerfeld integrals [Miller et al. (1977)]. This permitted evaluating the impedance-matrix coefficients for wire objects located on one side of an interface from simple bivariate interpolation, since the fields are then functions of only two variables, their lateral separation ρ and the sum of the vertical coordinates, z' and z, of the source and observations points relative to the interface, respectively. This essentially curve-fitting approach, used in NEC-2, reduced the matrix fill time to being little more than what is needed for a perfectly conducting ground where image theory is analytically rigorous. An example of the field variation on the same side of the interface as a fixed source located near an interface is shown as a function of observation position in Fig. 6. Clearly, the field is quite well-behaved and can be accurately approximated using linear interpolation.

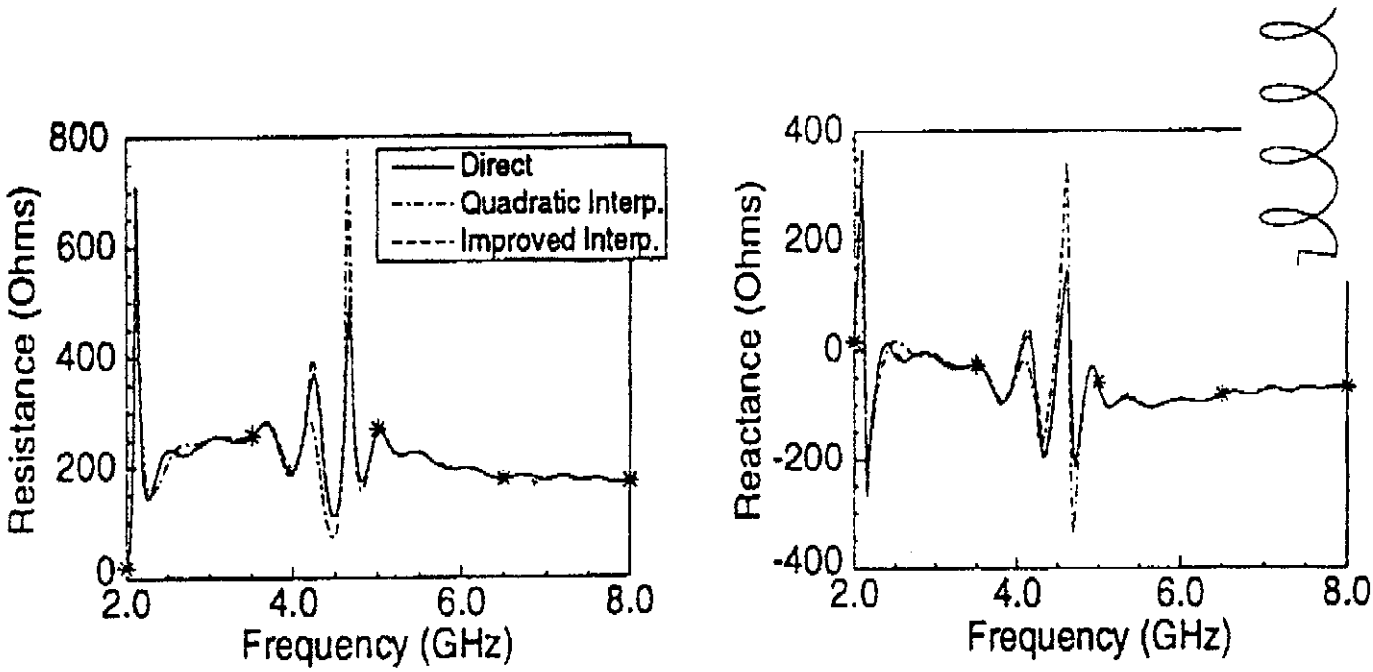

Figure 3. Results from using MBPE and two different FMs of the interaction coefficients of the $\underline{\underline{Z}}$ matrix for a helical antenna. Values obtained from straight-line interpolation of 301 GM samples (solid line) are compared with a quadratic FM (dot-dash line) and a FM defined by Eqs. (6) to (8) (dashed line) [Virga and Rahmat-Samii (1995)]. The GM samples used for the FM results are indicated by the starred points.

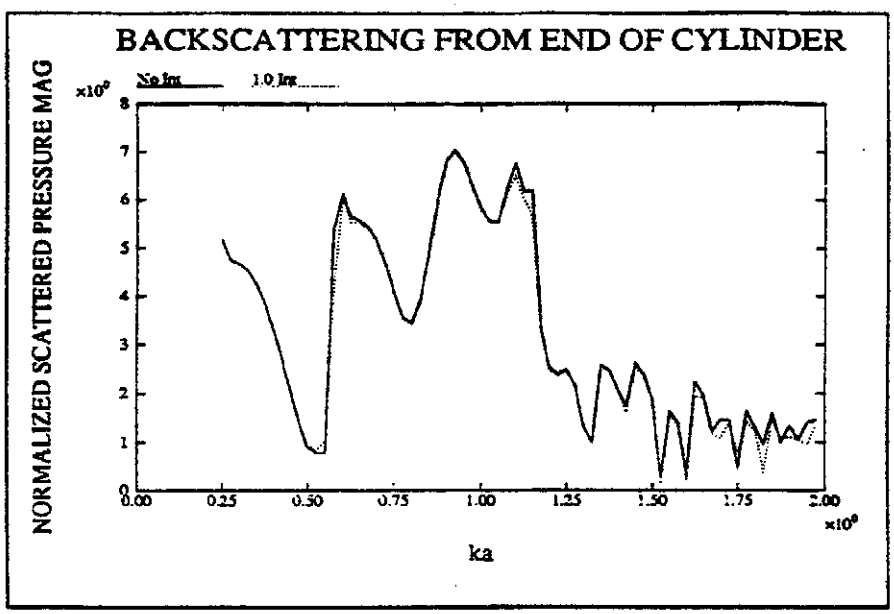

Figure 4. Results for acoustic backscattering from the end of a circular cylinder as a function of frequency obtained from the basic model without interpolation (solid line) and using MBPE on samples spaced 1.0 unit apart in ka (dotted line) [Benthien and Schenck (1991)]. A linear interpolation model is used for, $M_{m,n}(\omega_2 - \omega_1)$ in Eq. (6) to obtain the estimated interaction coefficients. The $\underline{\underline{Z}}$-matrix FM samples themselves are spaced too far apart to adequately resolve the fine structure of the response. A second series of pole-based FMs might be used to rectify this problem, as additional FM samples developed in the solution domain would require much less computation than using the formulation-domain FMs each of which involve solution of a large matrix.

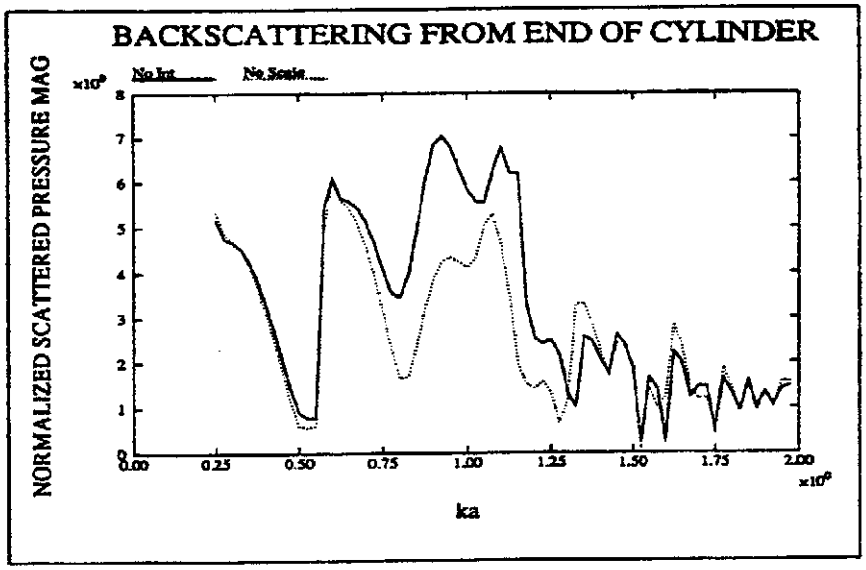

Figure 5. Results for acoustic backscattering from the end of a circular cylinder as a function of frequency obtained from the basic model without interpolation (solid line) and using MBPE on samples spaced 0.4 units apart in ka (dotted line) [Benthien and Schenck (1991)]. The Z-matrix interaction coefficients are estimated between their rigorously computed samples using a linear-interpolation model in Eq. (6), but absorbing the "scaling" factor, $\exp[j(\omega_2 - \omega_1)R_{m,n}/c]$, in $M_{m,n}(\omega_2 - \omega_1)$. Comparison of Figs. 5 and 6 emphasizes the importance of including the dominant functional variaions of the quantity being estimated in the MBPE process.

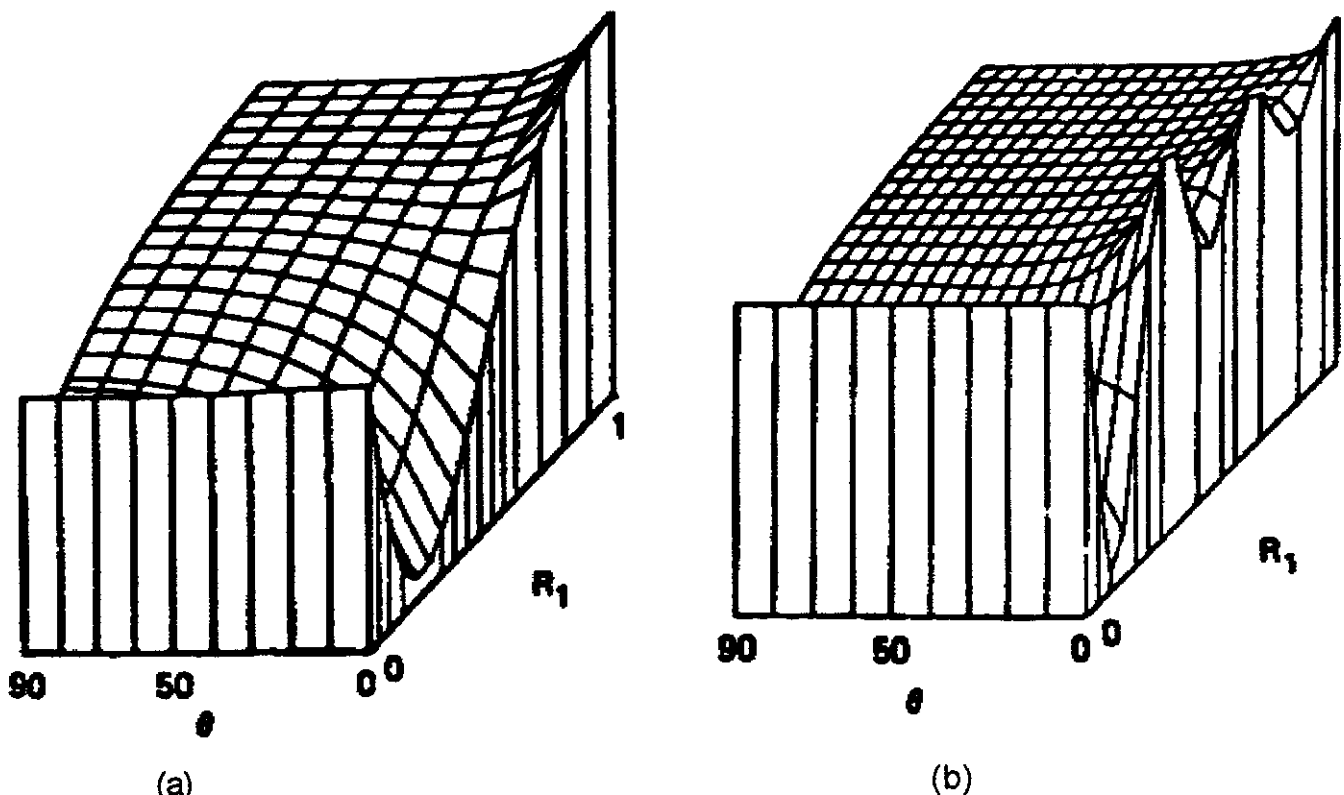

Figure 6. These plots exhibit representative electric fields due to a delta-current source located on the air side of an air-earth interface as a function of radial distance R_1 and elevation angle θ for a lossy, (a), and a lossless, (b), lower medium, respectively. The field is seen to be spatially less variable than the mathematical complexity of the Sommerfeld integral which gives it might imply. An interference between the different-wavelength above-surface and below-surface fields can be observed along the interface (where $\theta = 0$).

Later, in extending NEC-2 to model objects interacting across an interface, a problem where three-dimensional interpolation would have been required since the fields are then functions of lateral separation and the distance from the interface of both the source and observation point, an unattractive prospect, MBPE was then employed. The analytical "models" in this case are extracted from various asymptotic and other approximations that are applicable to the parameter range of interest so that Sommerfeld integrals of the form

$$V_{\pm}^{T} = 2\int_0^{\infty} \frac{e^{-\gamma_{-,+}|z'|-\gamma_{\pm}|z|}}{k_{-}^2\gamma_{+} + k_{+}^2\gamma_{-}} J_0(\lambda\rho)\lambda d\lambda, \quad (9)$$

are replaced by expressions like

$$\tilde{T}_{\rho}^{V} \approx \frac{-i\omega\mu_0 K}{4\pi}\left[\frac{k_{+}^2}{k_{+}^2 + k_{-}^2}\left(\frac{1-\sin\theta}{\cos\theta}\right) - S\cos\theta\right]R^{-1},$$

where

$$\theta = \tan^{-1}\frac{|z-z'|}{\rho},\ S = \frac{z'}{R},\ \text{and}\ K = \frac{k_{-}^2 - k_{+}^2}{k_{-}^2 + k_{+}^2} \quad (10)$$

with the details described by Burke and Miller (1984). Finally, the fields needed for the integral-equation model are then approximated by

$$E(r,z,z') \approx \sum A_n f_n(\rho,z,z');\ n = 1, \ldots, N \quad (11)$$

where the $f_n(\rho,z,z')$ functions comprise the model and A_n are the model parameters. This MBPE approach for the interface problem provides an essentially rigorous numerical model for objects interacting across an infinite, planar interface at a cost of increasing the matrix fill time by only 5-10 times over what modeling the same object(s) in free space would require. An example of one electric-field component transmitted to a lower medium from an above-surface source is shown in Fig. 7.

An alternate approach for the half-space problem based on a series of complex images developed using Prony's Method is described by Shubair and Chow (1993). For a verticallly oriented antenna, a series of three to five image antennas are found to be adequate for the one-sided problem (antenna on one side of the interface). A similar approach for a horizontal antenna is reported by Fang et al. (1988).

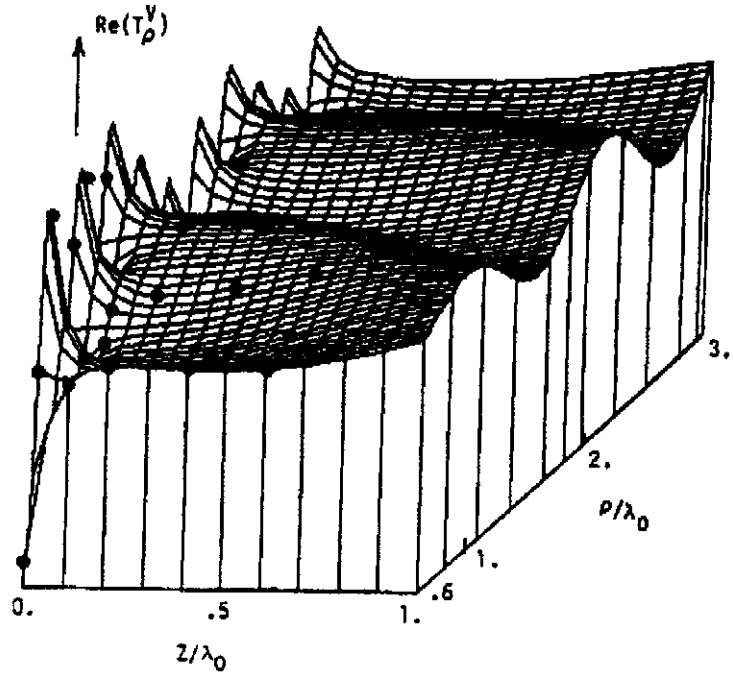

Figure 7. The MBPE FM results for the T_ρ^V field as a function of radial and vertical location beneath an interface for a source located above it [Burke and Miller (1984)]. Also shown by the dots are the Sommerfeld-integral values used as GMs for the FM approximation. Although not clearly shown because they overlap, the exact and MBPE results are both plotted in this figure.

4.1.4 Modeling Spatial Variations: Waveguide Fields.

Other opportunities for Green's-function applications of MBPE arise from separation-of-variables solutions for exterior problems involving cylinders, spheroids, etc. where infinite series of special functions occur and for interior problems where the Green's function can then involve an infinite series of images. An example of the latter application is reported by Demarest et al. (1989) for a wire antenna located in the region between infinite, parallel, perfectly conducting planes for which some results are shown in Fig. 8. The microscopic source-field description contained in the infinite-series Green's function for this problem is replaced by low-order FMs of the spatial field behavior that provide a much more efficient, yet acceptably accurate, numerical representation of these fields. These FMs substantially increase the efficiency of computing the interaction coefficients in an FDIE model by a factor of about 20 for the example shown. We note that the Green's function for this particular problem has the characteristics of both the WD and SD FMs, since the contribution of each image is pole-like, having a $1/(x - x_n)$ amplitude multiplied by a wave-like phase factor $\exp(-ik(x - x_n)$. The signal fields of this kind of Green's function might be described as having a hybrid character, with the goal of the FM being to replace both with a simpler analytical description.

4.1.5. Modeling Spatial Variations: Moment-Method Impedance Matrices.

The preceding examples deal with modeling the frequency variation of the coefficients of a FDIE system matrix as a means of reducing the number of needed FPM-matrix evaluations when spanning many resonances across some frequency band to reduce the overall operation count. Alternatively, we might examine the feasibility of reducing the number of FDIE-matrix coefficients that need FPM evaluation at a given frequency as way to reduce the OC at a given frequency. This kind of approach is described by Vecchi et al. (1994) and demonstrated by application to a microstrip line with a coupled dipole, an example of which is presented in Fig. 9. According to Vecchi et al., there is no appreciable difference between results obtained using the FM and the exact results.

Spatial variations of impedance and admittance matrices can be better appreciated by presenting them as surface plots, an example of which is included in Fig. 10a for a straight wire where the numbering of the subdomains used for this model is sequential from 1 to N. The axes represent the matrix rows and columns and the normalized height of the surface at row = m, column = n above the row-column plane represents the magnitude of a given interaction coefficient, $|Z_{m,n}|$. The plotting routine passes a smooth surface through the set of $|Z_{m,n}|$ values, and so may introduce a "fractional" interpolation between the discrete set of row-column indices. It's well-known, of course, that the impedance matrix for a straight wire or a strip is of Toeplitz form and so this particular matrix could be fully displayed by a single row or column. The matrix for the same wire bent to form a polygonal approximation of a circular loop would look very similar on this same linear scale except that there would be large components near the corners opposite the main diagonal, assuming the wire segments are numbered in order as well. Were a spatial FM to be used for these impedance matrices, the phase variation would also be needed, or as an alternative the real and imaginary parts might be used instead. The use of magnitude and phase for modeling $\underline{\underline{Z}}$ seems the more appropriate since they are "smoother" [Brown and Prata (1994)].

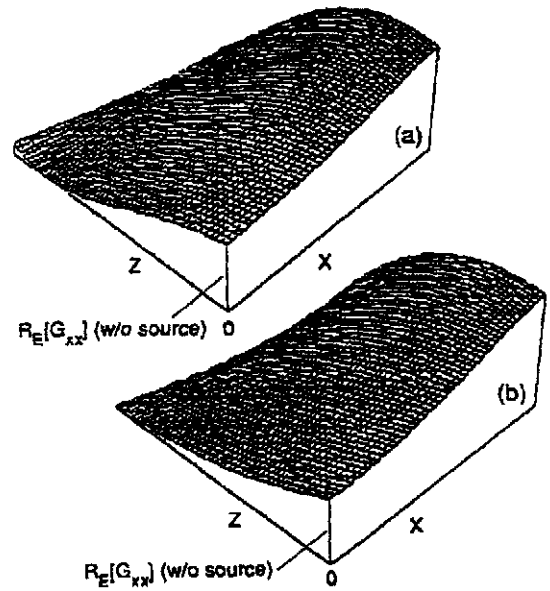

Figure 8. Results for the G_{xx} component of the dyadic Green's function (x-directed source perpendicular to waveguide walls, and x-directed field) as obtained from direct evaluation of the defining equation, (a), and as evaluated using a FM consisting of two multiplied 3rd-order polynomials in x and z, (b) [Demarest et al. (1989)]. The current on a dipole antenna located midway between the waveguide walls obtained from using (b) are within 5% of those resulting from (a).

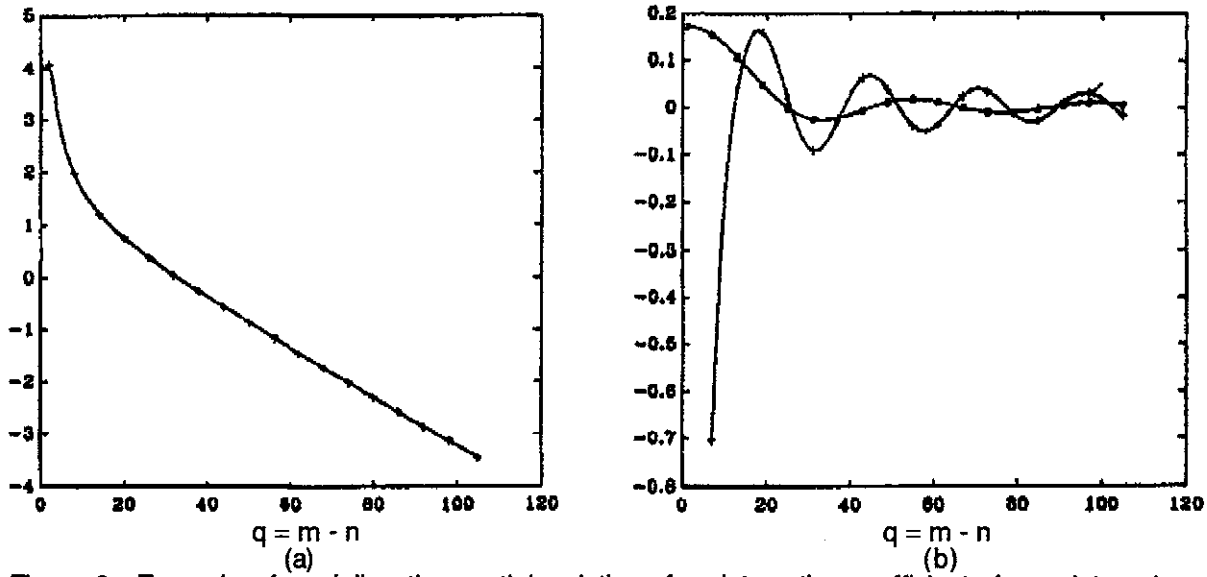

Figure 9. Example of modeling the spatial variation of an interaction coefficients for an integral-equation system matrix of a microstrip line with a coupled dipole using a Galerkin subdomain [Vecchi et al. (1994)]. Result in (a) is $\log_{10}$ of the static, singular part of the self-impedance matrix for the line as a function of the difference between the source and observation subdomain indices. The +'s show the points where the interactions are sampled for the FM, the solid line is the exact result and the dashed line is the FM result. The FM in this case is a polynomial applied to $Z_s[\log(q)]$. The results in (b) are obtained for the frequency-dependent part of the interaction coefficient, where the solid line is the exact result, the dashed line is FM approximation, again using a polynomial, and the o's and +'s indicate the real and imaginary samples used for evaluating the FMs.

An example for a more interesting structure, an 8-turn helical spiral having a total wire length of 16 wavelengths, is shown in Fig. 10b, also using a linear magnitude scale. A "splitting" of the coefficients along the main diagonal may be observed, due to the changing orientation of the neighboring wire segments as they spiral around the helix. This effect can be seen to continue as a ripple in the coefficients further away from the main diagonal.

More information is conveyed by plotting the log of the matrix coefficients, for which two examples are included in Fig. 11. The first, in (a), is for a wire two-free-space wavelengths in length, located parallel to, and 10^{-4} free-space wavelengths beneath, the interface between an upper free space and a lower half space having a relative dielectric constant of 10. There the interference between the waves propagating above and below the interface is seen in a somewhat different way than demonstrated in Fig. 6 for the Sommerfeld field alone. Aside from the fact that this matrix is also of Toeplitz form, and therefore more simply filled and solved than an arbitrary matrix, the regular variation of the coefficients in a given row or column indicates the feasibility of using a suitable spatial FM for reducing matrix-fill complexity.

When the same two-wavelength wire is rotated 90 degrees to penetrate the earth-air interface normally at its midpoint, the impedance matrix shown in Fig. 11b is obtained. The matrix is now block-Toeplitz but is otherwise nearly as simple spatially as is the case for the same object located in free space.

A much more complicated structure because it has a surface, rather than a linear, geometry is a wire mesh for which an impedance matrix is presented in Fig. 12. This plot dramatizes the problem encountered when attempting to visually display source-field relationships over a two-dimensional surface (or a three-dimensional volume) in terms of a two-dimensional matrix of interaction coefficients. The interactions are dependent on the four spatial coordinates that define observation- and source-patch locations Δ_m and Δ_n, respectively, as well on other details of the numerical model, and when projected onto the two-dimensional surface of the impedance matrix their associated spatial relationships are disordered. The field "signal" is no longer simply discerned by observing the behavior of a row or column from $\underline{\underline{Z}}$ but instead requires following a path through the matrix determined by the numbers assigned to the individual unknowns. This does not mean that the spatial variation of the fields can no longer be modeled, but that matrix indices can no longer serve as the FM variables.

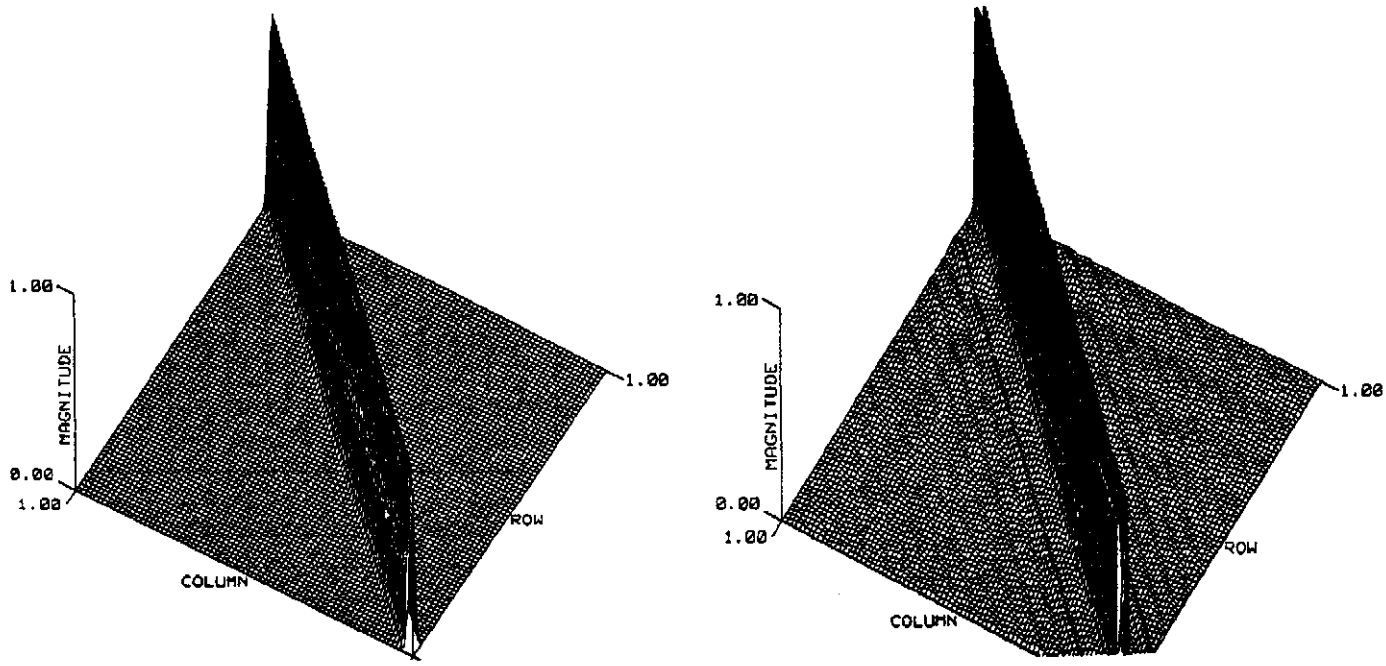

(a) (b)

Figure 10. Surface plots of the magnitudes of the impedance-matrix coefficients of a straight wire 2 wavelengths long, (a), and an 8-turn helical spiral 16 wavelengths long, (b).

4.2 Using Spectral MBPE in the Formulation Domain

A spectral FM would not be expected to be applicable to an integral equation based on a space-based Green's function, but could be appropriate for a transformed or modal Green's function where the variable is spatial wavenumber rather than distance. That possibility is not considered further in this discussion.

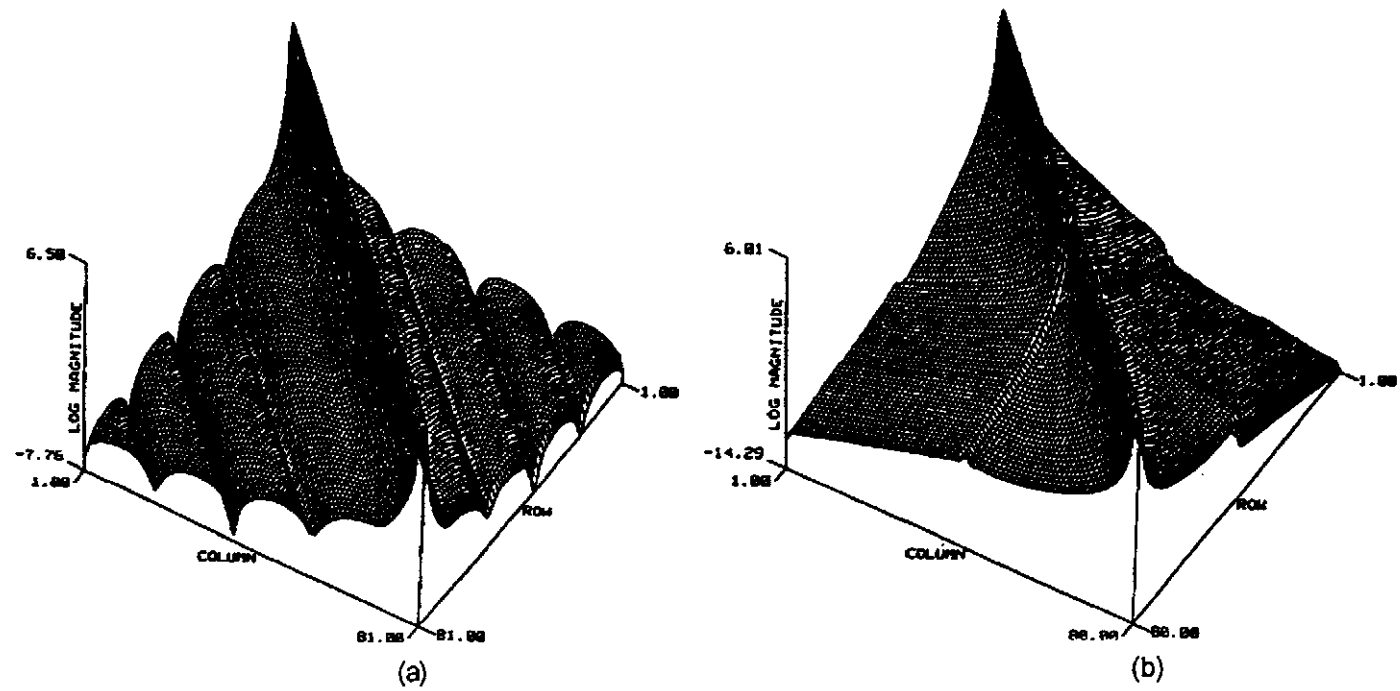

(a) (b)

Figure 11. Surface plots of the magnitudes of the impedance-matrix coefficients of a straight wire 2 wavelengths long in free space when parallel to, and 10^{-4} wavelengths beneath, an air-ground (ε_r = 10) interface, (a), and the same wire oriented normally to the interface with half its length in each half space, (b).

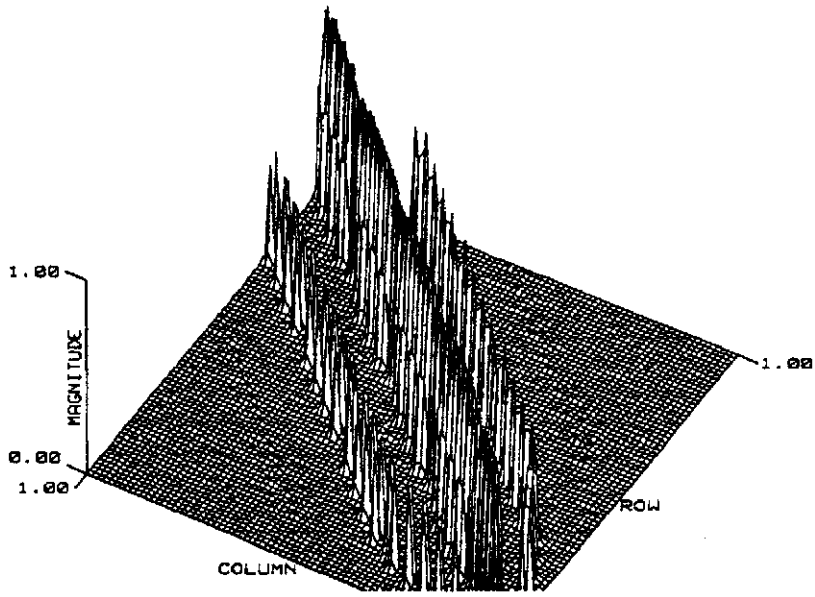

Figure 12. Surface plots of the magnitudes of the impedance-matrix coefficients of a 5-wire x 5 -wire mesh of wires whose total length is two wavelengths. The irregular appearance of this matrix results from the fact although the unknowns can be numbered in a sequential fashion, their separation is no longer linearly dependent on their respective indices.

5.0 SOLUTION-DOMAIN MBPE

5.1 Using Waveform MBPE in the Solution Domain

At least two kinds of CEM quantities in the solution domain possess wavelike nature, the source solutions themselves and the far-field angular dependence.

5.1.1 Modeling Spatial Variations.

While the spatial forms of the formulation-domain problem description provided by the impedance matrices are relatively uncomplicated, due to the basic simplicity of the Green's function source-field description, their solution-domain counterparts in the form of admittances matrices are not since the coefficients of the latter must encompass all possible source distributions that can occur on a given structure. Thus, whereas the impedance-matrix coefficients decline essentially monotonically with increasing distance, the admittance-matrix coefficients will in general not do this because, unless loss is a predominant effect, traveling-wave currents must be included among the distributions that can arise, becoming standing waves when impedance or other discontinuities occur on the structure being modeled. Never-the-less, the "signal" represented by the spatial variation of the induced sources, which is generally the current for conducting objects, is basically comprised of exponential waves and is therefore a potential candidate for MBPE using a WD FM. The potential significance of this possibility is that were a model for the spatial current response to be available, the number of parameters needed to quantify this current could be substantially less than the X_S coefficients otherwise used when developing an iterative solution, or the X_S^2 when the system matrix is factored. By combining iteration with MBPE of the spatial current, it may be feasible to obtain an acceptably accurate solution via iteration that requires ~ KX_S operations per iteration step rather than the X_S^2 normally involved, where K is the number of spatial current samples actually computed from the impedance matrix, an OC comparable to some of the "fast" methods mentioned above.

In order to explore the possibility of modeling the spatial variation of the admittance-matrix coefficients, a number of admittance-matrix, or $|Y_{i,j}|$, plots for some simple wire objects are plotted below.[1] The admittance

[1] Note that since the current on a structure represented by $\underline{\underline{Y}}$ is given by $\underline{I} = \underline{\underline{Y}} \cdot \underline{V}$, the current that results from exciting it as an antenna at a single point, or segment i = e, is $I_i = Y_{i,e} V_e$. Consequently, the current for this excitation is proportional to column "e" of the admittance matrix, and so as the excitation is scanned from e = 1 to e = X_S, the current that results can be discerned from observing the spatial behavior of column 1 to X_S of $|Y_{i,j}|$. We can thus refer to the plots of the admittance matrix as simply displaying its coefficients, or alternatively, a current distribution on the structure for which the matrix has been derived.

matrices for a two-wavelength straight wire and two-wavelength circular loop are shown in Fig. 13. It's clear in Fig. 13b for the loop that the spatial current is invariant in shape with respect to where the loop is excited, but simply rotates around the loop as the excitation point changes. It's not as clear, but suggestive from Fig. 13a for the straight wire, that the shape of its current distribution is also largely insensitive to where the the wire is excited, but that the magnitude of that current varies periodically with a changing excitation point. For these simple objects, it appears that not only might the current spatial dependence be described by a low-order, WD FM, but that, for the case of the straight wire, the dependence on excitation point can also be modeled.

Admittance-matrix plots for an 8-turn helix of total wire length 4 and 16 wavelengths, respectively, are shown in Fig. 14. The dramatic difference between the two results is due to the fact that in the former case, the helix is below cutoff because the circumference of the helical turns is less than a wavelength whereas the latter, being above the cutoff frequency, results in an attenuated traveling wave. Again, an exponential-series FM for the current appears to be a good approximation for either case.

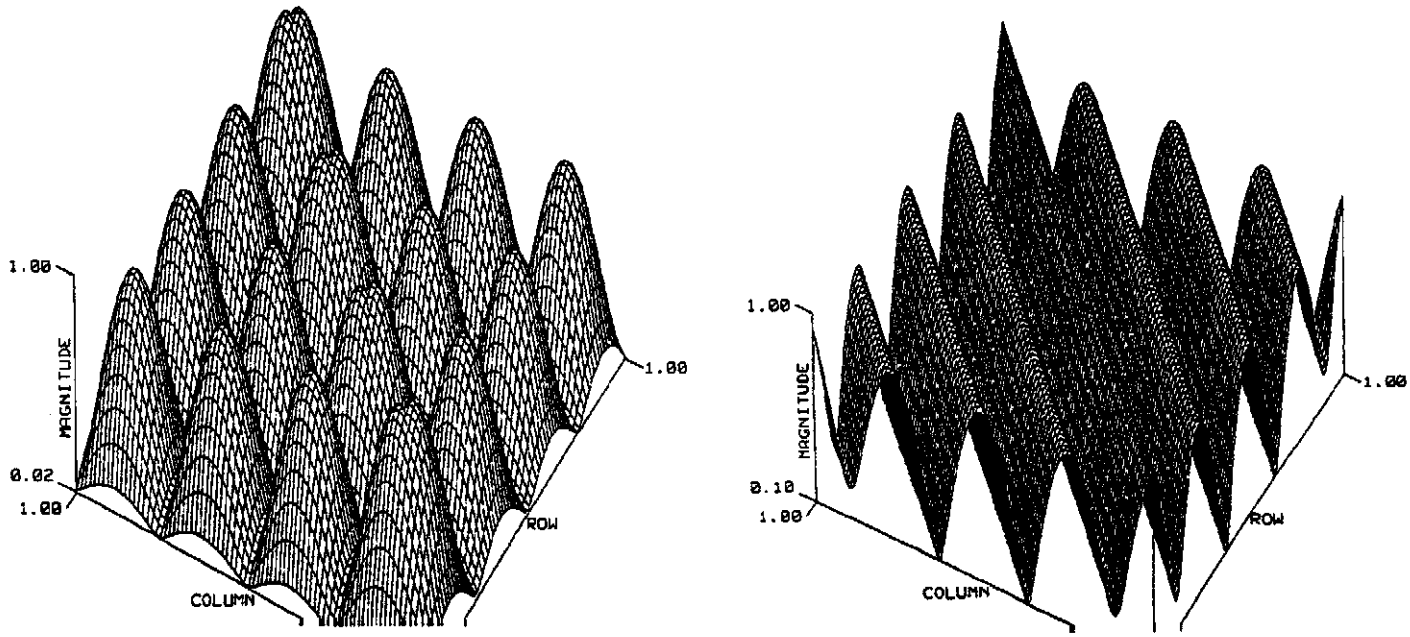

Figure 13. Surface plots of the magnitudes of the admittance-matrix coefficients of a two-wavelength-long straight wire, (a), and a circular loop, (b). Although the impedance-matrix magnitudes exhibit no explicit wavelength dependence (refer to the impedance matrix for the straight wire in Fig. 9a), the effects of standing waves are clearly evident in the admittance matrices. Also, whereas the field "signal" in the formulation domain, as represented by the impedance-matrix coefficients, falls off with distance, the corresponding current "signal" in the solution domain, does not necessarily do so, instead exhibiting the propagating-wave nature expected on such structures.

The plots in Fig. 15 show the magnitudes of the admittance matrix coefficients for a wire two-free-space-wavelengths long that is parallel to, and 10^{-4} wavelengths above and 10^{-4} wavelengths beneath, the interface between free space and a dielectric half space of $\varepsilon_r = 10$. The transition between a spatial current distribution having a dominant wavelength characteristic of free space and that of the dielectric is seen to occur over a very small vertical movement of the wire.

The results of Fig. 16 are for the same horizontal wire as Fig. 15a but with a half-space relative permittivity of $\varepsilon_r = 10 - j10$, (a), and for the two-wavelength wire oriented perpendicular to the interface with its midpoint at the interface, (b). The effect of the half-space loss on the horizontal-wire current distribution of part (a) is seen to cause an increased attenuation, which, in terms of a exponential-series FM indicates that the effective wavenumber has developed a larger real part. In Fig. 16b, the vertical wire can be seen to carry two distinctly different current waves on each half having a wavelength appropriate to the medium in which that wire half is located. For the cases of Figs. 15 and 16, an exponential-series FM for the current would again seem to be a good approximation.

The final result of this sequence, Fig. 17, is the admittance matrix of the wire mesh whose impedance

matrix is shown in Fig. 12. Not unexpectedly, there is no discernible pattern in this plot for the reasons previously stated. Both the graphical presentation of such matrices for two-dimensional surfaces and the associated FMs needed for their spatial modeling would need to take into account their higher-order dimensionality, as compared with the one-dimensional nature of wires.

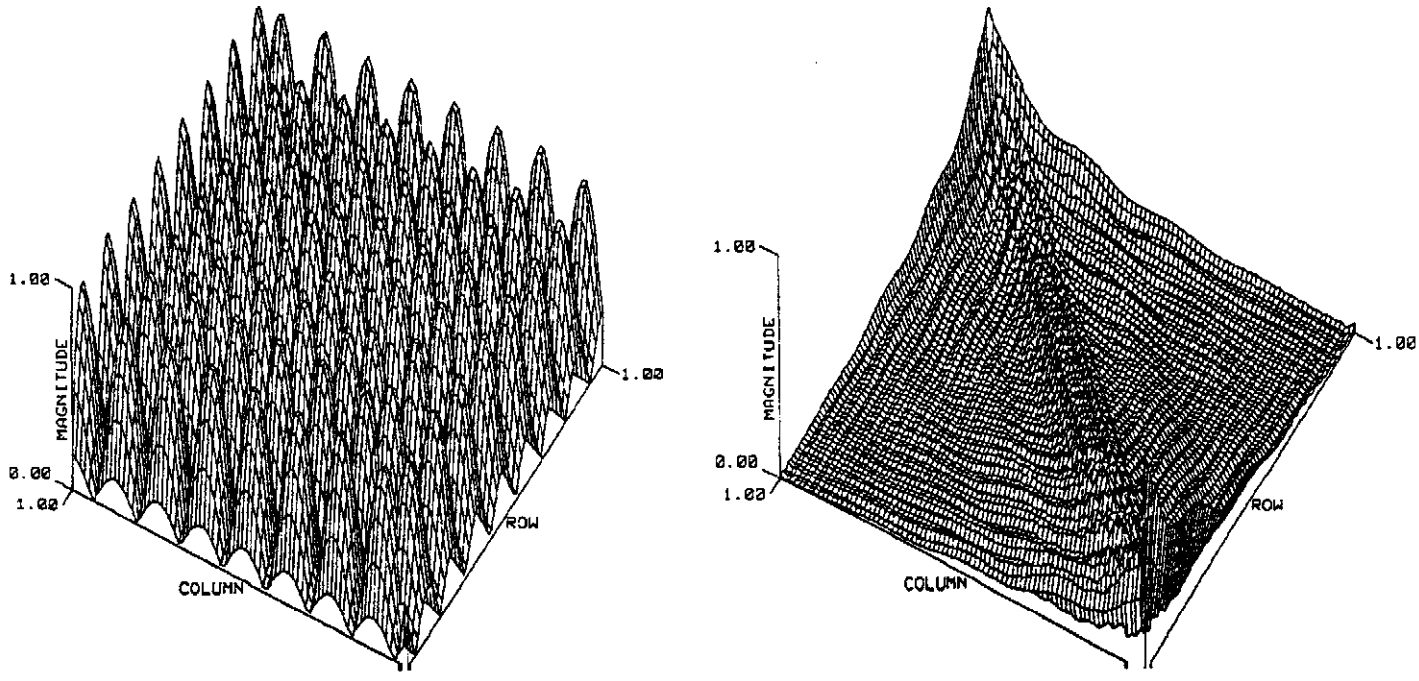

(a) (b)

Figure 14. Surface plots of the magnitudes of the admittance-matrix coefficients for an 8-turn helix of total wire length 4 wavelengths, (a), and 16 wavelengths, (b). In (a), the structure is below cutoff since the helix circumference, C, is less than λ, whereas for (b), C ~ 2 λ, so that the dominant current behavior changes from a standing wave to a damped traveling wave.

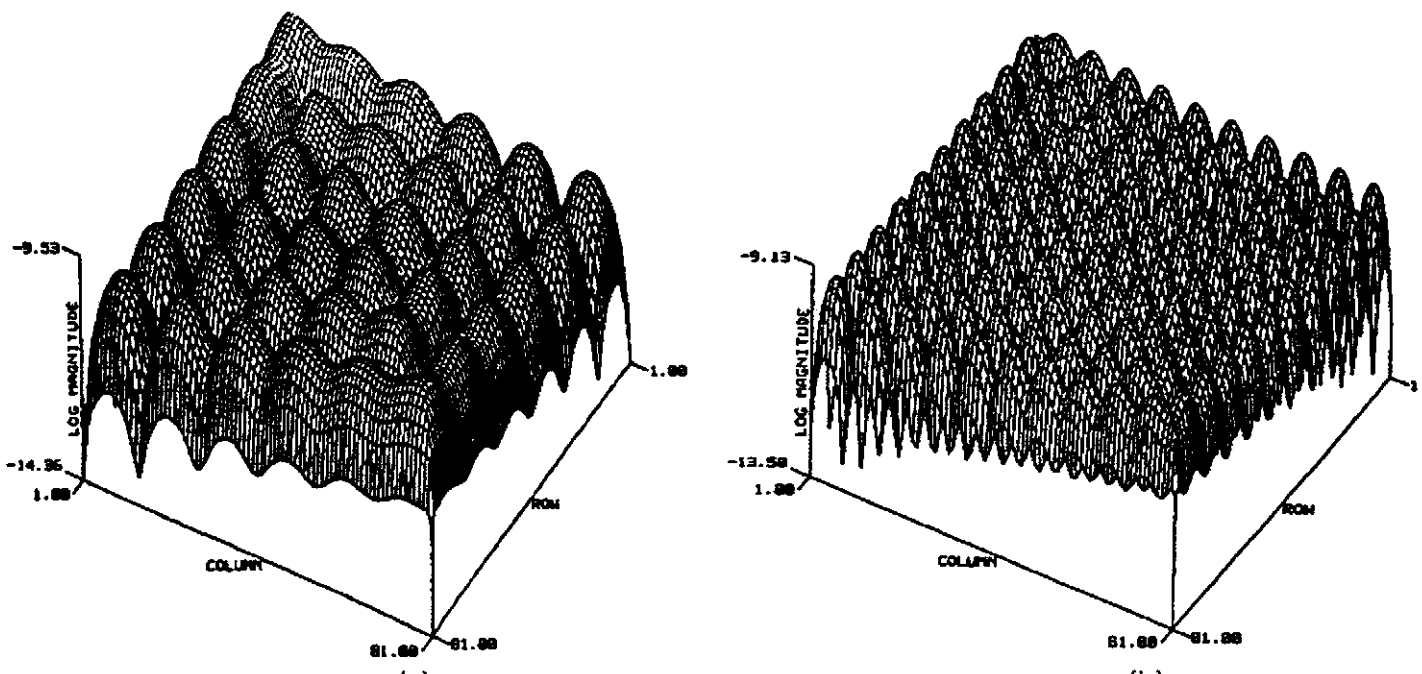

(a) (b)

Figure 15. Surface plots of the magnitudes of the admittance-matrix coefficients for a two-wavelength (in free-space) wire parallel to a dielectric half-space of ε_r = 10 when 10^{-4} wavelengths above the interface, (a), and 10^{-4} beneath the interface, (b). The damped, standing-wave nature of the current is again evident, with a change from the free-space value to the half-space value taking place over a vertical distance of ~ 10^{-4} wavelengths, or less.

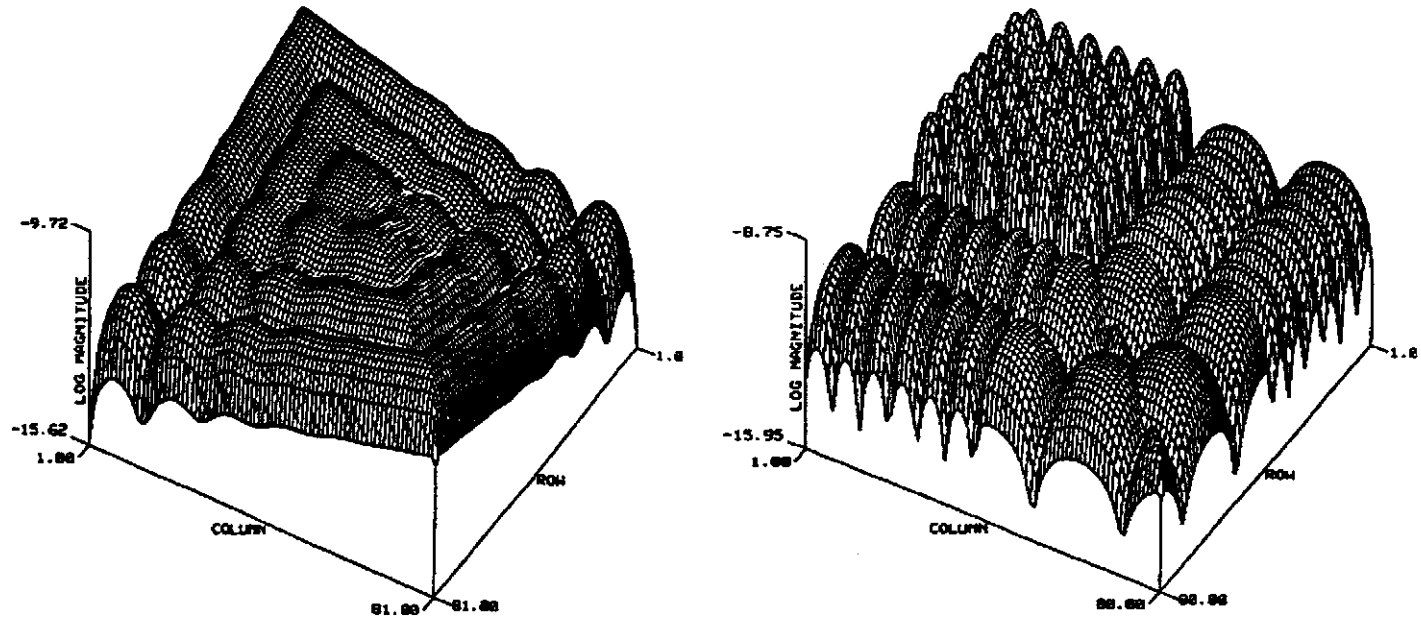

Figure 16. Surface plots of the magnitudes of the admittance-matrix coefficients for a two-wavelength wire in free space when parallel to and 10^{-4} free-space wavelengths above a half space with $\varepsilon_r = 10 - j10$, (a), and for the same wire when perpendicular to a dielectric half space of $\varepsilon_r = 10$ with its center at the interface, (b). The influence of the lossy lower half space is evident in the increased current attenuation exhibited in (a) as compared with 15a. The change in dominant current wavelength in the vertical wire is clearly demonstrated in (b) on each half of the wire. Again, an appropriate Fitting Model for such currents is an exponential series, or waveform-domain, form.

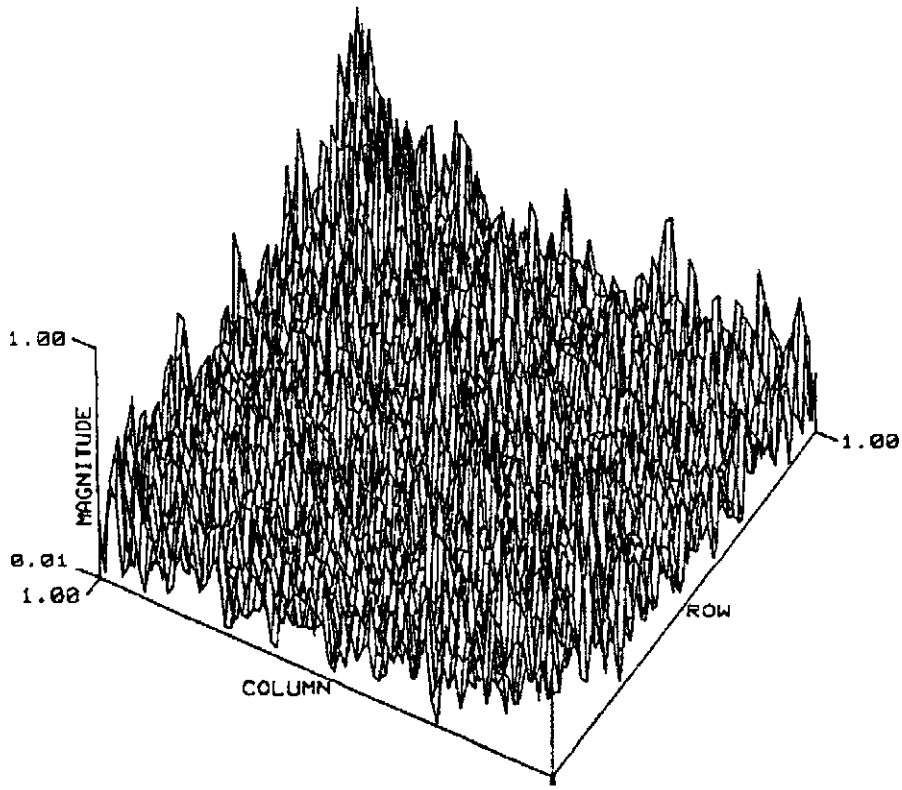

Figure 17. Surface plot of the magnitudes of the admittance-matrix coefficients for a 5-wire x 5 -wire mesh of wires whose total length is two wavelengths. The irregular appearance of this matrix results from the fact although the unknowns can be numbered in a sequential fashion, their separation is no longer linearly dependent on the respective indices used to construct the system and solution matrices.

5.1.2 Modeling Angle Variations of the Far Field. The far-field approximation universally used to obtain the distant field of a known source distribution depends only on the angular coordinates of the far-field observation point relative to the coordinate-system origin and the source location projected onto the line-of-sight from that origin. For a simple linear array of discrete sources, the far electric field a can be expressed in the general form

$$E(\theta) \approx \sum S_n \exp[ikd_n \cos(\theta)];\ n = 1, \ldots, N \tag{12}$$

where S_n and d_n are, respectively, the amplitude and location along the array of source n of which there are a total of N. The radiation pattern is normally developed by sampling the far fields finely enough in angle such that a straight-line interpolation between the field samples can be employed to develop an approximation continuous in observation angle. Clearly, Eq. (12) has the form of an exponential series and is a candidate for a WD FM. Two- and three-dimensional source distributions have a more complicated far-field expression, but otherwise retain the basic structure of Eq. (12), being functions of two observation angles, elevation and azimuth in a spherical coordinate system.

For extended source distributions, where N exceeds 50 or so, it is not computationally practical to employ a single FM for the entire pattern since ill-conditioned data matrices are encountered. Furthermore, a pattern that is a function of two angles can not be directly modeled using the basic Prony model described in RI. Instead, observation windows of limited angular extent can be used so that low-order FMs can accurately approximate the pattern over that window. The pattern can then be developed by employing enough FMs so that a continuous range of observation angles is encompassed over the angle variations that are desired. This approach has been described by Roberts and McNamara (1994) and is summarized in RI.

5.2 Using Spectral MBPE in the Solution Domain

In RI, the use of FMs to represent the frequency dependence of EM observables was discussed and demonstrated using various examples. Here we consider the more fundamental problem of modeling the frequency dependence of the admittance matrix itself using both function sampling and derivative sampling.

5.2.1 Modeling the Admittance Matrix. As previously discussed, the impedance or system matrix arising from an FDIE model contains all the interaction information needed to describe the EM properties of an object being modeled. In a numerical model, this information is represented by the fields produced at observation patches in response to unit-amplitude source patches, both sets of which span the entire object. The relative amplitudes and phase-changes associated with the X_S^2 source-field patch pairs convey object size implicitly in these interactions. The inverse of these relationships in the form of the admittance matrix is needed to establish the absolute source amplitudes that satisfy the required boundary conditions. The solution, or admittance, matrix explicitly includes aspects of object size and shape the effects of which are exhibited as periodic body resonances as a function of frequency. Thus, the model appropriate for MBPE representation of the admittance matrix must be capable of handling frequency-dependent resonances.

Since the observables that the solution matrix provides are well-approximated by pole series, or more generally rational functions, as demonstrated in RI, it follows that the solution matrix itself might also be modeled using rational functions. This conclusion follows by noting that for a single-port antenna its input admittance is defined as the ratio of the feedpoint current to the exciting voltage. For a wire antenna excited at segment j then, having already shown that the admittance can be modeled by a rational function, the $Y_{j,j}$ coefficient of the solution matrix must also have this model. Similarly, the currents on the other wire segments for that excitation, given by $Y_{i,j}$ where $i = 1, \ldots, i-1, i+1, \ldots, X_S$ if there are a total X_S segments, can also be modeled using a rational function. These observations extend to exciting other segments of the wire one at a time, indicating that each coefficient in the solution matrix can be represented by a rational-function FM. Furthermore, since each of these coefficients shares the same resonance structure and thus the same denominator polynomial, the solution matrix can be modeled by a denominator polynomial multiplying a matrix of numerator polynomials, as exhibited by

$$\underline{Y}(s) = \frac{1}{D(s)} \begin{bmatrix} X & \cdots & X & n_{1a}(s) & \cdots & n_{1b}(s) & \cdots \\ X & \cdots & X & n_{2a}(s) & \cdots & n_{2b}(s) & \cdots \\ X & \cdots & X & n_{3a}(s) & \cdots & n_{3b}(s) & \cdots \\ \vdots & \vdots & \vdots & \vdots & \vdots & \vdots & \vdots \\ X & \cdots & X & n_{X_s a}(s) & \cdots & n_{X_s b}(s) & \cdots \end{bmatrix} \tag{13}$$

where $n_{i,j}(s)$ is the numerator polynomial for coefficient i,j, D(s) is the common denominator and a and b are the indices of those excitation ports whose current response have been modeled. This form permits direct representation of the wire current for an arbitrary right-hand-side excitation so long as its frequency lies within the valid bandwidth of the solution matrix or of the rational function FMs that comprise its coefficients.

5.2.2 Sampling Admittance-Matrices Derivatives. The FM approaches discussed here for estimating frequency responses require sampled values of the impedance or admittance matrices from which the MBPE parameters can be computed and from which the FM is thus quantified. The sampling can be done either as a function of frequency; as a function of derivative, with respect to frequency at a given frequency; or a combination thereof Miller and Burke (1991). Also, since an EM frequency response has complex-conjugate behavior around zero frequency, this knowledge can be employed to provide virtual samples that further improve the MBPE performance, i.e., negative-frequency samples can be employed at essentially no further FPM cost.

For practical reasons of numerical conditioning and accuracy, however, it is advisable not to cover too-wide a frequency interval with a single model. The approach that now seems most attractive is to employ a series of frequency windows that slide over the frequency interval to be modeled. These windows can be of lower order to avoid the conditioning problems that can otherwise. Using sliding, and overlapping, windows also can yield some estimate of the numerical accuracy of the modeled transfer function by comparing the results of two, or more, windows in their region of overlap where they share common samples, some examples for which are included in RI. Here, we outline specifically the additional computational benefits that arise from derivative sampling.

On writing the moment-method equations that arise from an integral-equation formulation in matrix form, the impedance equation

$$\sum_{i=1}^{X_s} Z_{i,j}(\omega) I_j(\omega) = V_i(\omega) \tag{14}$$

is obtained where these various quantities are evaluated at the frequency ω. A solution for the current can then be formally written as an admittance equation

$$I_i(\omega) = \sum_{j=1}^{X_s} Y_{i,j}(\omega) V_j(\omega) \tag{15}$$

where $Y_{i,j}$ is the inverse of $Z_{i,j}$. We should note however that the approach developed here for the frequency derivatives could be implemented using LU factorization, iteration, or any other solution method.

Upon differentiating the impedance equation with respect to frequency there is obtained

$$\sum_{j=1}^{X_s} [Z_{i,j}(\omega) I_j'(\omega) + Z_{i,j}'(\omega) I_i(\omega)] = V_i'(\omega) \tag{16}$$

where the prime denotes a frequency derivative. A solution of the differentiated impedance equation for the differentiated current can then be written

$$I_i'(\omega) = \sum_{j=1}^{X_s} Y_{i,j}(\omega) \left(V_j'(\omega) - \sum_{k=1}^{X_s} Z_{j,k}'(\omega) I_k(\omega) \right) \tag{17}$$

where we observe that while the differentiated impedance matrix appears as part of a modified right-hand-side of the differentiated admittance equation, I' is given in terms of an undifferentiated admittance matrix. Computing the differentiated current thus requires an additional number of computations beyond those needed for solution of the undifferentiated current proportional to X_S^2 rather than the X_S^3 that would apply to obtain another frequency sample (assuming that LU decomposition is used rather than iteration).

Continuing this process, the n'th frequency derivative of the current is given by

$$I_i^{(n)}(\omega) = \sum_{j=1}^{X_s} Y_{i,j}(\omega)\left[V_j^{(n)}(\omega) - \sum_{m=1}^{n} C_{nm}\left(\sum_{k=1}^{X_s} Z_{jk}^{(m)}(\omega) I_k^{(n-m)}(\omega) \right) \right] \tag{18}$$

where again $C_{n,k}$ is the binomial coefficient and the superscript in parenthesis indicates differentiation with respect to frequency of the order indicated.

It is especially important to observe that information about the n'th frequency derivative of the current continues to require an operation count proportional to X_S^2. Expressed in another way, each additional frequency derivative of the solution vector for the current can be computed in a number of operations proportional to $A(n,N_{rhs})/X_S$ where A is a function which depends on the order of the derivative and the number of right-hand-sides for which the solution is sought. If the frequency derivatives provide information comparable to that available from the frequency samples themselves, it can be appreciated that there could be a substantial computational advantage to using the solution derivatives in estimating the transfer functions. The problem of mplementing the above approach in the NEC code is discussed by Miller and Burke (1991).

6.0 CONCLUDING COMMENTS

The applicability of low-order fitting models (FMs) in computational electromagnetics both to reduce the sampling density of computed observables and to decrease the computational cost of obtaining these observables has been the focus of this and a companion article [RII, Miller (1995)]. Both of these possibilities rest on the fact that much EM modeling is redundant, in that source and field variations as a function of time, frequency, angle and space can be accurately described by physically derived FMs that permit equivalent information to be determined from fewer computations. A conclusion to be reached from this observation is that first-principles models (FPMs) need not be employed in the manner they most often now are to obtain desired information. Rather, supplementary information is available from our knowledge of EM mathematics and physics, allowing us to employ reduced-order models to represent observables obtained from a FPM or to reduce the complexity of the FPMs themselves. This substitution offers the possibilities of greatly decreasing the number of evaluations required of FPMs and the cost of their evaluation, with a consequent reduction in the overall computer cost required to obtain the information desired.

In the context of using an FDIE solved using the moment method, modeling the frequency variation of the impedance matrix saves an operation count (OC) proportional to X_S^2 for each frequency sample that can be eliminated. Similarly, modeling the frequency variation of the admittance matrix produces an OC savings proportional to X_S^3 for each sample eliminated. Modeling the spatial variation of the impedance matrix can reduce the OC of a solution towards $X_S \log(X_S)$, which forms the basis for the newer, "fast" techniques. Modeling the spatial variation of the admittance matrix might offer similar kinds of savings, but has not yet been tested. For problems solved using a FPM and requiring hours of computer time for each new frequency sample, the savings in computer resources resulting from matrix modeling can be substantial. The models discussed, especially for the admittance matrix, not only provide a more useful representation of the physical behavior continuous in the independent variable, but are valuable for other purposes such as obtaining transient responses.

7.0 ACKNOWLEDGEMENT

The author gratefully acknowledges the contributions of G. J. Burke and J. K. Breakall in providing the matrix plots used in this article.

8.0 REFERENCES

Benthien, G. W. and H. A. Schenck (1991), "Structural-Acoustic Coupling," in *Boundary Element Methods in Acoustics*, ed. R. D. Ciskowski and C. A. Brebbia, Computational Mechanics Publications.

Brown, K. W. and A. Prata (1994), "Efficient Analysis of Large Cylindrical Reflector Antennas Using a Nonlinear Solution of the Electric Field Integral Equation," IEEE Antennas and Propagation Society International Symposium, Seattle, WA, pp. 42-45.

Burke, G. J. and E. K. Miller (1984), "Modeling Antennas Near to and Penetrating a Lossy Interface", *IEEE Transactions on Antennas and Propagation*, **AP-32**, pp. 1040-1049.

Burke, G. J. and E. K. Miller (1988), "Use of Frequency-Derivative Information to Reconstruct an Electromagnetic Transfer Function," *Proceedings of the Fourth Annual ACES Review*, Naval Postgraduate School, Monterey, CA, March.

Burke, G. J., E. K. Miller, S. Chakrabarti, and K. Demarest (1989), Using Model-Based Parameter Estimation to Increase the Efficiency of Computing Electromagnetic Transfer Functions," *IEEE Trans. Magnetics*, **Vol. 25**, No. 4, pp. 2807-2809, July.

Canning, F. X. (1990), "Transformations That Produce a Sparse Moment Matrix", *J. Electromagnetic Waves and Applications*, **4**, pp. 983-993.

Chew, W. C. (1993), "Fast Algorithms for Wave Scattering Developed at the University of Illinois' Electromagnetics Laboratory," *IEEE Antennas and Propagation Magazine*, **35**, no. 4, pp. 22-32.

Coifman, R., V. Rokhlin and S. Wandzura (1993), "The Fast Multipole Method for the Wave Equation: A Pedestrian Prescription," *IEEE Antennas and Propagation Magazine*, **34**, no. 3, pp. 7-12.

de Beer, J. T. and D. C. Baker (1995), "An Examination of the Effect of Mechanical Deformation on the Input Impedance of HF LPDA's Using MBPE", *Appled Computational Electromagnetics Society Journal*, this issue.

Demarest, K. R., E. K. Miller, K. Kalbasi, and L-K Wu (1989), "A Computationally Efficient Method of Evaluating Green's Functions for 1-, 2-, and 3D Enclosures", *IEEE Transactions on Magnetics*, **25**(4), pp. 2878-2880.

Fang, D. G., J. J. Yang, and G. L. Delisle, (1988), "Discrete Image Theory for Horizontal Electric Dipoles in a Multilayered Medium," *IEE Proceedings*, **135**, pp. 297-303.

Miller, E. K. (1995), "Model-Based Parameter Estimation in Electromagnetics: I--Background and Theoretical Development," *Applied Computational Electromagnetics Society Newsletter*, submitted for publication.

Miller, E. K. (1996), "Model-Based Parameter Estimation in Electromagnetics: II--Applications to EM Observables," *Applied Computational Electromagnetics Society Newsletter*, submitted for publication.

Miller, E. K., J. N. Brittingham, and J. T. Okada (1977), "Bivariate- Interpolation Approach for Efficiently and Accurately Modeling Antennas Near a Half Space", *Electronics Letters*, 13, pp. 690-691.

Miller, E. K., F. J. Deadrick, G. J. Burke and J. A. Landt (1981), "Computer-Graphics Applications in Electromagnetic Computer Modeling, *Electromagnetics*, 1, pp. 135-153.

Miller, E. K. and G. J. Burke (1991), "Using Model-Based Parameter Estimation to Increase the Physical Interpretability and Numerical Efficiency of Computational Electromagnetics," Computer Physics Communications, **68**, pp. 43-75.

Newman, E. H. (1988), "Generation of Wide band Data From the Method of Moments by Interpolating the Impedance Matrix," *IEEE Trans. Antennas Propagat.*, Vol. 36, No. 12, pp. 1820-1824.

Oppenheim, A. W. and R. W. Schafer (1975), *Digital Signal Processing*, Prentice-Hall, Inc., Englewood Cliffs, NJ.

Ralston, A. (1965), *A First Course in Numerical Analysis*, McGraw-Hill Book Co.

Roberts, A. R. and D. A. McNamara (1994), "Interpolating Radiation Patterns Using Prony's Method," in *Proceedings of Symposium on Antennas and Propagation and Microwave Theory and Techniques*, University of Stellenbosch, Stellenbosch, South Africa, October, pp. 151-154.

Shanks, Daniel (1955), "Non-Linear Transformations of Divergent and Slowly Convergent Sequences," *Journal of Mathematics and Physics*, the Technology Press, Massachusetts Institute of Technology, Cambridge, MA, pp. 1-42.

Shubair, R. M. and Y. L. Chow (1993), "A Simple and Accurate Complex Image Interpretation of Vertical Antennas Present in Contiguous Dielectric Half-Spaces," *IEEE Transactions on Antennas and Propagation*, **AP-41**, pp. 806-812.

Vecchi, G., P. Pirinoli, L. Matekovits and M. Orefice (1993), "Singular Value Decomposition in Resonant Printed Antenna Analysis," in *Proceedings of Joint 3rd International Conference of Electromagnetics in Aerospace Applications*, pp. 343-346.

Virga, K. and Y. Rahmat-Samii (1995), "Wide-Band Evaluation of Communications Antennas Using [Z] Matrix Interpolation with the Method of Moments," in *IEEE Antennas and Propagation Society International Symposium*, Newport Beach, CA, pp. 1262-1265.